Journal Pre-proof

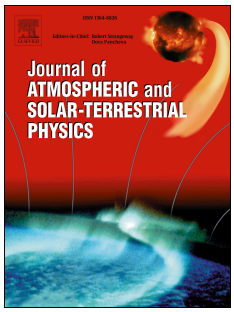

IMF By-Driven Electric Field Disturbances Over the Equator During Northward IMFs: PPEF Responses

Ram Singh, Tarun Kumar Pant, S. Sripathi, D. Rout, A. Bhaskar, Danny E. Scipion

PII: S1364-6826(25)00226-3

DOI: https://doi.org/10.1016/j.jastp.2025.106642

Reference: ATP 106642

To appear in: *Journal of Atmospheric and Solar-Terrestrial Physics*

Received Date: 12 June 2025

Revised Date: 10 September 2025

Accepted Date: 15 September 2025

Please cite this article as: Singh, R., Pant, T.K., Sripathi, S., Rout, D., Bhaskar, A., Scipion, D.E., IMF By-Driven Electric Field Disturbances Over the Equator During Northward IMFs: PPEF Responses, *Journal of Atmospheric and Solar-Terrestrial Physics*, https://doi.org/10.1016/j.jastp.2025.106642.

IMF By-Driven Electric Field Disturbances Over the Equator During Northward IMFs: PPEF Responses

Ram Singh[1, 2,] Tarun Kumar Pant[2], S. Sripathi[3], D. Rout[4], A. Bhaskar[2], and Danny E. Scipion[1]

[1]Radio Observatorio de Jicamarca, Instituto Geofísico del Perú, Lima, Peru
[2]Space Physics Laboratory, Vikram Sarabhai Space Centre, Trivandrum, India
[3]Indian Institute of Geomagnetism (IIG), New Panvel, Navi Mumbai, India
[4]National Atmospheric Research Laboratory, Gadanki, India,

Corresponding author: Ram Singh (ramphysics4@gmail.com)

Abstract

This article provides the first evidence of equatorial and low-latitude ionospheric electric field disturbances driven by quasi-periodic variations in the interplanetary magnetic field (IMF) By component, under a constant northward IMF Bz (~+15 nT), solar wind dynamic pressure (~8 nPa), solar wind velocity (~450 km/s), and positive Sym-H (+10 nT). The virtual height of the F layer (h'F), measured by ionosondes at opposite longitudes in the American (Jicamarca, 11.9°S, -76.0°E; Fortaleza, 3.9°S, -38.52°E) and Indian (Trivandrum, 8.5°N, 77.0°E; Tirunelveli, 8.73°N, 77.7°E) sectors, shows electric field disturbances with opposite polarities during the day and night, driven by changes in the IMF. During northward IMF Bz conditions, vertical E×B plasma drifts measured by the Jicamarca Incoherent Scatter Radar (ISR), along with equatorial electrojet (EEJ) observations, reveal westward electric field disturbances on the dayside. Conversely, on the nightside, ionosonde measurements at Trivandrum and Tirunelveli show eastward electric field perturbations. Notably, quasi-periodic electric field fluctuations with prominent periodicities of approximately 15 minutes are observed in both the IMF By and ionospheric parameters, such as dh'F/dt and EEJ, in both local time sectors. These fluctuations are most likely driven by modulations in high-latitude disturbance polar (DP2) currents. SuperDARN ionospheric convection maps display enhanced convection, rotation, and expansion, which appear to influence the equatorial electric field. The presence of northward Bz (NBZ) currents and reverse convection patterns likely contributes to the observed westward electric field perturbations at low latitudes.

Keywords

Interplanetary Magnetic field (IMF) By, Prompt Penetration Electric field (PPEF), Equatorial Ionosphere, Northward Bz currents (NBz), Vertical Plasma Drift.

1. Introduction

The enhanced magnetospheric convection electric field, generated by the interaction between the solar wind and the magnetosphere, significantly influences ionospheric electrodynamics during magnetic storms (e.g., Nishida, 1968a; 1968b; Kelley, 1979; Tsurutani et al., 2004, 2008; Mannucci et al., 2005b). Under southward IMF Bz conditions, the dawn-to-dusk electric field (IEFy), also known as the convection electric field, rapidly penetrates into the ionosphere. The propagation of the transverse magnetic mode (TM_0) in the Earth-ionosphere waveguide plays a key role in facilitating this penetration from high to low latitudes (e.g., Kikuchi et al., 1978; 1996). In the equatorial ionosphere, this penetrating electric field exhibits an eastward (dawn-to-dusk) polarity during the day and a westward (dusk-to-dawn) polarity at night. When the IMF Bz turns northward, the magnitude and direction of the convection electric field begin to weaken, and an overshielding electric field develops within the plasmasphere. The polarity of this overshielding field is eastward at night and westward during the day (e.g., Fejar et al., 1979; Kelley et al., 1979; 2007; Kikuchi et al., 1996**;** Tsurutani et al., 2004, 2008; Huang, 2009, 2012; Baskar and Vichare, 2013).

Kelley et al. [1979] introduced the concept of under- and over-shielding of the magnetospheric electric field, focusing on how the Alfven layer, a boundary region near the edge of the ring current, controls the transmission of electric fields from the magnetosphere to the inner magnetosphere and ionosphere. Under-shielding happens during the early stages of a geomagnetic disturbance (e.g., southward turning of IMF), when the shielding currents in the inner magnetosphere (especially the ring current and Region 2 field-aligned currents) have not yet fully developed. In this case, magnetospheric penetration electric fields (such as those from solar wind-magnetosphere interactions) can reach low-latitude ionospheric regions with little attenuation, causing prompt penetration electric field (PPEF). Over-shielding, on the other hand, occurs during the recovery phase of geomagnetic activity (e.g., northward turning of IMF) when shielding currents still persist even after the external driver (like the solar wind electric field) has decreased or stopped. In the ionosphere, this results in electric fields of opposite polarity due to an overshoot of the shielding effect. Over time, studies have been built on this idea, using observational data and modeling to measure the presence and effects of

penetration electric fields on equatorial ionospheric dynamics, including the EEJ and ionospheric plasma drifts (e.g., Fejer and Scherliess 1997; Tsurutani et al., 2004, 2008; Kelley et al., 2007; Huang, 2009; Singh et al., 2024, 2025; Rout et al., 2025). Huang (2009) presented that the observed westward penetrating fields during substorm onset are likely due to the associated overshielding effects, rather than the substorm itself. Under steady southward IMF Bz conditions, substorms have been shown to induce eastward penetrating electric fields in the low-latitude ionosphere (e.g., Huang, 2012). The penetration of IMF components into the magnetosphere occurs under various orientations, not only during southward IMF. Tsurutani et al. (1984) found that roughly 13 % of the IMF By component is transmitted into the magnetotail, implying that the same physical mechanisms that drive interplanetary electric-field penetration are at work.

Another type of penetration known as the DP2 (disturbance polar current) type penetration, occurs when IMF Bz oscillates in the north and south directions. When DP2-type electric field perturbations occur, the ionospheric electric field and magnetometer data reflect similar types of periodic changes from high to lower latitudes (e.g., Nishida, 1968a, 1968b; Sastri et al., 2000; Huang, 2019a, 2020; Singh et al., 2022; Rout et al., 2022). Aside from these electric field perturbations, studies have revealed that the electric field penetration in low latitude ionosphere may be triggered by several types of source mechanisms, including magnetic substorms and a sudden increase in solar wind pressure (e.g., Wei et al., 2009; Rout et al., 2016; Huang, 2020; Singh & Sripathi, 2021). A few studies have also shown the electric field penetration associated with IMF By across equatorial and low-latitude ionosphere (e.g., Kelley and Makella, 2002; Chakrabarty et al., 2017; Hui and Vichare, 2021; Kumar et al., 2023). Kelley and Makella (2002) first reported the IMF By associated penetration electric over low-latitude ionosphere using vertical plasma drift measurements. Hui and Vichare (2021) suggested utilizing the TIEGCM model that under IMF Bz southward conditions, the polarity of IMF By can considerably affect electric field penetration and neutral dynamics. It is important to mention here that these studies have shown the impact of the IMF By over low latitude ionosphere under the southward IMF Bz conditions. Therefore, it is yet to be investigated the effects of IMF By on the low latitude ionospheric electric field during the northward IMF Bz conditions.

This study aims to investigate the electrodynamic response of the equatorial and low-latitude ionosphere to periodic changes in the IMF By component under conditions of steady northward IMF Bz. It is important to highlight that previous research has primarily focused on the effects

of IMF By during southward IMF Bz conditions, which are typically associated with enhanced magnetospheric convection and prompt penetration electric fields (e.g., Kelley and Makela, 2002; Chakrabarty et al., 2017). However, to the best of the authors' knowledge, no systematic study has been conducted to investigate how periodic oscillations in IMF By influence the penetration of electric fields over the low-latitude ionosphere during steady northward IMF Bz conditions. This study provides the first observational evidence of ionospheric disturbances linked to penetrating electric fields driven by IMF By fluctuations during sustained northward IMF Bz. Through the combination of measurements from opposite longitude sectors (both from India and American longitude), the study aims to reveal new insights into the magnetosphere-ionosphere coupling mechanism.

The structure of this study is as follows: Section 2 describes the source of data analysis. Observations and results are presented in Section 3. Section 3.1 contains the solar wind geomagnetic conditions, and Section 3.2 presents the ground-based measurements. Sections 4 and 5 provide the discussion and conclusion.

2. Data Sets

In this study, we used digisonde and Canadian Advanced Digital Ionosonde (CADI) data to calculate the F-layer height (h'F) and rate change of height (dh'F/dt) at Jicamarca (JIC: 11.9°S; - 76.8°E), Fortaleza (FTZ: 3.9ºS, -38.52ºE), Trivandrum (TVM: 8.5°N; 77°E), Tirunelveli (TIR: 8.73° N, 77.70° E), and Guam (GUA: 13.69°N; 144.87°E) stations. The Jicamarca Incoherent Scatter Radar (ISR) recorded vertical plasma drift measured by the JULIA MP (Jicamarca Unattended Long-Term Investigations of the Ionosphere and Atmosphere Medium Power) mode was also used. The time interval for JULIA radar data was 5 minutes, whereas the ionograms on the FTZ and JIC were recorded at 10- and 15-minute intervals, respectively. The ionogram intervals at TVM, TIR, and GUA were 7, 10, and 15 minutes, respectively. The local times at the locations are given by LT = UT+5.5 hours (at TVM and TIR), LT = UT+9.6 hours (at GUA), LT = UT-5 hours (at JIC), and LT = UT-3 hours (at FTZ). The two magnetometers located at equatorial and off-equatorial sites at Jicamarca (1.9°S, 76.8°W, ~0.5°N dip latitude) and Piura (5.2°S, 80.6°W, ~6.81°N dip latitude) are used to calculate the EEJ. The EEJ is a key feature of low-latitude electrodynamics. It is influenced by both external factors, such as IMF-driven electric fields, and internal drivers like tidal winds and conductivity variations (e.g., Zhang et al., 2021). The EEJ consists of a narrow band of intense eastward current flowing in the E-region ionosphere. It is typically confined within ±3° magnetic latitude of the magnetic equator and occurs at an altitude of

approximately 100–110 km. The solar wind parameters are obtained from ACE satellite measurements, and the geomagnetic indices are sourced from WDC Kyoto. A global network of real-time magnetic observatory magnetometers is used to acquire magnetic field data. SuperDARN observations are used to generate convection maps of the Northern Hemisphere at high latitudes.

3. Observations and Results

3.1 Solar Wind and Geomagnetic Conditions

The interplanetary and geomagnetic conditions on December 19, 2015, between 15:00 and 20:00 UT are presented in Figure 1. The change in solar wind speed (Vsw, red), solar wind dynamic pressure (Pdyn, black), and particle density (Np, green) are shown in Figure 1a. Figures 1b-1h show variations in IMF Bx, By, and Bz, IEFy, auroral electrojets (AU and AL), and Sym-H. Except for the IMF By component interplanetary and geomagnetic conditions, no significant changes were exhibited between 16:30 and 18:00 UT, as shown in the grey shaded area. Interestingly, under steady northward Bz (~ +15 nT) conditions, and with stable values of Vsw, Np, and Pdyn at 450 km/s, 20 cm^{-3}, and 8 nPa, respectively, the IMF By fluctuated between ±8 nT, showing three significant peaks. Positive and negative peaks were noticed at 16:55 and 17:06 UT, 17:12 and 17:20 UT, and 17:27 and 17:35 UT, respectively. At the same time, Sym-H expressed an eastward ring current with a value of nearly +10 nT. The positive and negative values of By correspond to the dusk and dawn side polarities of the magnetic field. It must be noted that this observation is unique as it has been found after carefully analyzing more than 30 years of solar wind data. Figure 2 shows the changes in energetic particle fluxes (e.g., electron flux) between 15:00 and 20:00 UT. The electron fluxes were detected at different energy levels (i.e., 40, 75, 150, 275, 475 keV) by nine telescopes (numbered 101-109) on geosynchronous satellites (GOES-13 and 15). The left panels show observations from GOES-13, while the right panels display observations from GOES-15. The magnetic footpoints of GOES-13 and 15 were located at Geog: 57.5°N, 79.2°W and 59.5°N, 129.2°W, respectively. Dispersonless particle injection at geosynchronous was not observed during the noon (between 01:34 and 12:56 MLT) and morning (between 07:35 and 08:55 MLT) hours. The GOES 13 shows a dispersion less particle injection at 18:30-19:00 UT (09:25-09:55 MLT), but the location and local time duration do not coincide with our results. However, AU/AL (Figure 1e) also did not observe any substorm signatures; the initial increase in particle injection at 16:15 UT (Figure 2) appears to be caused by a rise in solar dynamic pressure (Figure 1e).

3.2 Ground-based Ionosonde and Radar Observations over Indian and American Longitudes

Figure 3 shows ground-based ionosonde observations over the Indian longitudes during nighttime hours between 15:30 and 19:00 UT (21:00 and 00:30 LT). Figures 3a, 3b, and 3c illustrate the virtual height (h'F) variations, as well as the mean and standard deviation estimated from five International Quiet Days (IQDs) for Guam, Tirunelveli, and Trivandrum, respectively. Figure 3d depicts the vertical plasma drift (dh'F/dt), which is derived using the rate of change in ionospheric height (i.e., F-layer height) at Trivandrum. Figure 3e lists variations in IMF By (blue) and Bz (red). Interestingly, the h'F and dh'F/dt variations shown in the vertical cyan shaded regions coincide well with IMF By changes and exhibit quasi-periodic oscillations, similar to IMF By between 16:45-18:00 UT. The time resolution and data intervals are not the same in each observation. Ionosonde observations from Tirunelveli and Guam stations are used to validate Trivandrum observations. The h'F enhancements and oscillations in virtual height and vertical plasma drift within the shaded region could be attributed to disturbances in the eastward electric field. Notably, the vertical plasma drift and virtual height at the dip equator indicate the presence of an eastward electric field rather than the typically expected westward field during nighttime hours.

Figure 4 presents ionosondes, ISR radar, and magnetometers observations during daytime hours over the American longitude sector, along with IMF data. Figure 4a and 4b show variations in the ionospheric virtual height (h'F) along with the five-day mean and standard deviation of IQD variations at the Jicamarca and Fortaleza stations, respectively. Figure 4c presents the vertical plasma drift (Vd) measured by the Jicamarca ISR operating in JULIA MP mode (black circles), along with the drift predicted by the Scherliess and Fejer (SF) model, represented by the black line (e.g., Fejer & Scherliess, 1997). Figure 4d presents the EEJ together with its five-day IQD mean and standard deviation. Figure 4e displays variations in the IMF components By (blue) and Bz (red), as well as the detrended ΔEEJ (green). The ΔEEJ is calculated by subtracting the mean EEJ values from the event-specific EEJ values The vertical plasma drift, EEJ, and virtual height exhibited a sudden increase caused by the eastward enhanced electric field generated by the southward IMF Bz at ~16:20 UT. Afterward, the ISR drift and EEJ showed a steady reduction in their values due to the westward electric field between 16:35 and 18:05 UT, corresponding to a steady northward IMF Bz. However, during this constant reduction, the ISR drift and EEJ exhibited oscillations corresponding to the IMF By. Subsequently, a sudden increase was observed in the ISR drift, EEJ, and h'F,

corresponding to the southward IMF Bz between 18:00 and 18:30 UT.

Notably, the vertical plasma drift, EEJ, and h'F (at Jicamarca) exhibit a significant reduction compared to the quiet-time mean variations. This reduction is attributed to the westward prompt penetration electric field, which opposes the background eastward field, leading to the observed decrease between 16:35 and 18:00 UT (Figures 4b, 4c, and 4d). On the dayside, the eastward penetration electric fields are not strong enough to fully cancel the westward electric field, allowing the westward electric field oscillations to persist. The ionosonde measurements from Fortaleza further confirm the electric field disturbance, as significant oscillations in h'F are evident (Figure 4a). The clear oscillations in the westward electric field disturbance are shown in ΔEEJ, which closely follow the IMF By oscillations (Figure 4e). These findings support a correlation between IMF By variations and the oscillations observed in the EEJ, vertical plasma drift, and h'F, driven by IMF By. The disturbed electric field oscillations associated with IMF By fluctuations are highlighted in the cyan-shaded region.

To understand the ionospheric perturbations in the electric field carried by IMF By reorientations, Figure 5 illustrates a periodogram analysis using the Lomb-Scargle (LS) method and Morlet wavelet analysis (e.g., Lomb, 1976; Torrence and Compo, 1998) for IMF By, EEJ, and dh'F/dt at Trivandrum. The left panels show the LS periodogram, the middle panels show the wavelet spectrogram, and the right panels show the global wavelet spectrum (GWS). The third-order Savitzky-Golay smoothing algorithm was used to eliminate the long-term fluctuations for the periodogram analysis (e.g., Savitzky & Golay, 1964; Singh et al., 2022). The LS periodogram analysis and GWS reveal a dominant common periodicity of ~15 minutes in the ionospheric parameters, as well as in the IMF By. Wavelet analysis demonstrated spectral power enhancements centred at periods of around 15 minutes and showed common periodicity. According to this analysis, the reorientations of the IMF By by carrying out electric field circumstances are substantially triggering the common periodic oscillations in the ionosphere.

Figure 6 provides the DP2 contours and convection maps at the following times: (a) 17:00-17:02 and 17:06-17:08 UT; (b) 17:18-17:20 and 17:20-17:22 UT; and (c) 17:26- 17:28 and 17:30-17:32 UT. The contour maps with polar cap potentials are shown in the supporting Figure (S). From the Figures, it can be seen that reverse convection or NBZ (northward Bz-component) currents exist when the IMF By polarity is negative or in the dusk direction (Figure 6a, 6c, and S); during the IMF By positive condition, the NBZ currents are very weak. The convection cell grew larger toward lower latitudes and rotated toward

the dawnside during the time of positive IMF By (Figure 7b and S).

4. Discussion

The region-1 (R1) and region-2 (R2) field-aligned currents (FACs) system and related magnetospheric plasma convection are driven by the dynamic interaction of the solar wind and the magnetosphere. R1, R2, and their horizontal currents produce the DP2 (disturbance polar current) current system at high latitudes, create an extra electric field there, and undergo large changes with changes in the IMF Bz (e.g., Kikuchi et al., 1978; 1996). In the plasma sheet, the magnetospheric convection electric field (dawn to dusk potential drop) gets stronger under the southward IMF Bz condition. This enhanced convection electric field subsequently interacts with the high-latitude ionosphere, causes disruption to the DP2-type current system, and promotes the DP2-type current system to reach lower latitudes instantly (e.g., Nishida, 1968a, 1968b; Kikuchi et al., 1996). In the local noon hours, an additional current system that exists just poleward of the R1 FACs occurs at times of almost entirely northward IMF Bz and is referred to as NBZ (northward Bz) or cusp currents (e.g., Iijima and Potemra, 1978), or sunward convection (e.g., Vasyliunas, 1989; Vennerstrom et al., 2002). The NBZ current system is composed of two localized FAC regions that are symmetrically positioned at local noon in both hemispheres and move in the opposite direction compared to R1 FACs, which enter and exit the ionosphere on the dawn and dusk sectors. The IMF By causes large asymmetries in the magnetosphere that are reflected in global currents, convection patterns, and auroral intensity by changing the flow of plasma in both hemispheres in various ways (e.g., Weimer, 1995, 1996). In our observations on the dayside, the eastward enhanced electric field was caused by the southward turning of IMF Bz (e.g., Tsurutani et al., 2004; 2008; Fejar et al., 1979), which enhanced the EEJ, increased the vertical plasma drift, and raised the F-layer height over the American longitudes, as shown in Figure 4 at around 16:20 and 18:05 UT (e.g., Singh et al., 2024, 2025; Rout et al., 2025). At the same time, on the nightside over Indian longitudes, a reduction in h'F was observed, which was caused by the westward penetration electric field (Figure 3).

Figures 3 and 4 exhibited eastward (on the nightside, between 21:30 and 23:00 LT) and westward (on the dayside, between 11:30 and 13:00 LT) electric field penetration signatures over Indian and American longitudes, respectively. These penetration electric fields with opposite polarity are caused by reverse convection or NBZ currents (e.g., Huang, 2019a). In our observations, Figures 6a and 6c demonstrate the formation of reverse convection and NBZ currents. Huang (2019a) observed a westward penetration electric field on the dayside

and suggested that reverse convection and NBZ currents are the main generators for this electric field. Figure 6 displays the ionospheric convection maps in the northern hemisphere made by the SuperDARN of HF (high frequency) radars between 17:00 and 17:32 UT under the constant northward IMF Bz condition, attempting to understand the electric field penetration driven by IMF By. Arrows in the SuperDARN convection maps indicate convection vectors computed from the radar echoes, while contours in the maps display statistical data. The convection maps show the occurrence of reverse convection (sunward) or NBZ currents within the polar region. Figures 6a and 6c show ionospheric convection maps at 17:00, 17:06, 17:26, and 17:32 UT when IMF By turns from positive to negative (dawn to dusk) direction or is in duskside (e.g., negative By). Most importantly, as the reverse convection occurs, dusk and dawn cells split into multiple cells and shift towards lower latitudes. The westward and eastward electric field disturbances are observed at the equator on the dayside and nightside. These penetrating electric fields are generated by reverse convection or NBZ current as reported by Huang (2019a).

According to Heelis (1984), significant changes in the interplanetary magnetic field (IMF) By can effectively modify the DP2 currents, causing them to expand toward lower latitudes. The size and morphology of the convection cells in the morning and evening sectors are controlled by both the magnitude and direction of IMF By and Bz, as well as by distortions in the DP2 current pattern induced by IMF By fluctuations (e.g., Heelis et al., 1982; Heelis, 1984; Ruohoniemi and Greenwald, 2005; Tenfjord et al., 2015). Previous studies have investigated how the IMF influences high-latitude plasma convection and DP2 currents (e.g., Heelis, 1984; Ruohoniemi and Greenwald, 2005; Tanaka, 2007).

In our observations, under positive IMF By (i.e., duskward By perturbations), the dusk cell extended toward the dayside and adopted an approximately circular shape, whereas the dawn cell assumed a crescent shape (Figure 6b). Simultaneously, the overall convection pattern rotated clockwise about the noon midnight meridian, yielding anticlockwise plasma flow in the nightside sector and a duskward zonal flow near midnight. Conversely, for negative IMF By (i.e., dawnward By perturbations), the dawn cell became nearly circular and the dusk cell became crescent-shaped; the entire pattern again rotated clockwise, producing dawnward zonal flow at midnight (Figures 6a, 6c). These distortions in the polar convection cells appear to be regulated by fluctuations in IMF By under sustained northward Bz conditions, thereby triggering oscillations in the equatorial electric fields.

The periodic oscillations of disturbance electric fields, driven by various solar wind

magnetosphere interaction processes, have been extensively investigated in earlier studies (e.g., Nishida, 1968a, 1968b; Sastri et al., 2000; Huang, 2019a; Singh et al., 2022; Rout et al., 2022). Near the magnetic equator, Nishida (1968a, 1968b) reported quasi-periodic oscillations in the geomagnetic field recorded by ground-based magnetometers, which coincided with IMF Bz fluctuations. Subsequent studies have identified a broad range of periodicities associated with DP2-type electric field fluctuations, including 25–35 minutes (e.g., Sastri et al., 2000), 30–40 minutes (e.g., Kikuchi et al., 1996; Chakrabarty et al., 2015), 40 minutes (e.g., Raut et al., 2019), and dual periodicities of 30 and 60 minutes (e.g., Rout et al., 2017; Singh et al., 2022). In this study, we report for the first time a DP2-type fluctuation with a 15-minute periodicity, which appears to be linked to fluctuations in the IMF By component. Figure 5 reveals a consistent and dominant 15-minute periodicity in IMF By, EEJ, and d'F/dt at both longitudes. These shared periodicities between IMF By and ionospheric parameters suggest that DP2-associated perturbations influence the equatorial electric field. Owing to the rotation and expansion of the dawnside convection cell, both the dayside (Jicamarca) and nightside (Trivandrum) stations observed these electric field oscillations, indicating a longitudinally coherent response (e.g., Chakrabarty et al., 2017).

5. Summary

This study highlights the dominant role of the IMF By in causing the electric field disturbances in the ionospheric system at opposite longitude sectors at the same time. During northward IMF Bz, the westward electric field in the dayside equatorial zone should be seen as coming from two separate sources: reverse convection (e.g., Huang et al., 2019a) in the polar region and R-2 FACs (e.g., Kikuchi et al., 1978; 1996). Conversely, the polar reverse convection can be responsible for transmitting the westward electric field. In our case, the opposite polarity of the disturbed electric fields observed at equatorial latitudes is most likely driven by NBZ currents, rather than by R2 FACs, which typically occur at much lower latitudes. However, the similar oscillatory behavior in the disturbed electric fields appears to result from the combined effects of strong convection, enlargement, and rotations of the convection cells. Under constant northward IMF Bz conditions, a DP2-type prompt penetration electric field of 15-minute periodicity is found to be observed in IMF By, ionospheric vertical plasma drift, and the EEJ. The southward turning of the IMF Bz heightened the dayside eastward electric field, which strengthened the EEJ, increased vertical plasma drift, F-region virtual height, and the nightside westward electric field disturbance.

6. Acknowledgements

This work was initiated during a Research Associateship (RA) fellowship at the Indian Space Research Organization (ISRO) and finalized at the Jicamarca Radio Observatory in Lima, Peru. The Jicamarca Radio Observatory is a facility of the Instituto Geofísico del Perú, operated under an agreement with Cornell University through Prime Agreement AGS-2213849 from the National Science Foundation. RS acknowledges the financial support provided through the RA fellowship by ISRO, Department of Space, Government of India. We express our sincere gratitude to the teams of ACE, SuperDARN, JULIA radar, and ionosonde for their valuable contributions. The authors also acknowledge the use of SuperDARN data. SuperDARN is a global network of radars supported by national scientific funding agencies in Australia, Canada, China, France, Italy, Japan, Norway, South Africa, the United Kingdom, and the United States. We are grateful to the Low-Latitude Ionospheric Sensor Network (LISN) for providing magnetometer data.

Declaration of Competing Interest

The authors declare that they have no known competing financial interests or personal relationships that could have appeared to influence the work reported in this paper.

Data Availability Statement

The Jicamarca Radio Observatory's Madrigal Database provided the JULIA radar data used in this study (http://jro1.igp.gob.pe/madrigal/). The Jicamarca Radio Observatory is a facility run by the Instituto Geofisico del Peru with funding from the NSFAGS-1433968 through Cornell University. Data for the interplanetary and geomagnetic conditions were obtained from the NASA GSFC CDAWeb (http://cdaweb.gsfc.nasa.gov/istp_public/) and WDC kyoto (http://wdc.kugi.kyoto-u.ac.jp). The international real-time magnetic observatory magnetometer network (https://imag-data.bgs.ac.uk/GIN_V1/GINForms2) was used to gather magnetic field information. The convection maps were downloaded from SuperDARN Network (https://superdarn.ca/). The Global Ionosphere Radio Observatory (GIRO) online provides access to the ionosonde data at https://giro.uml.edu/didbase/.

References

Bhaskar, A., and G. Vichare (2013). Characteristics of penetration electric fields to the

equatorial ionosphere during southward and northward IMF turnings J. Geophys Res. Space Physics, 118, 4696-4709, doi:10.1002/jgra.50436.

Chakrabarty, D., D. Hui, et al. (2017). Role of IMF By in the prompt electric field disturbances over equatorial ionosphere during a space weather event, J. Geophys Res. Space Physics, 122, 2574–2588, https://doi.org/10.1002/2016JA022781.

Fejer, B. G., and Scherliess, L. (1997). Empirical models of storm time equatorial zonal electric fields. J. Geophys. Res., 102 (A11), 24047– 24056, doi:10.1029/97JA02164.

Fejer, B., Gonzales, C., Farley, D., Kelley, M., & Woodman, R. (1979). Equatorial electric fields during magnetically disturbed conditions the effect of the interplanetary magnetic field. J. Geophys. Res., 84(A10), 5797–5802.

Heelis, R. A. (1984). The effects of interplanetary magnetic field orientation on the dayside high latitude convection. J. Geophys. Res., 89, 2873–2880.

Heelis, R. A., Lowell, J. K., & Spiro, R. W. (1982). A model of the high latitude ionospheric convection pattern. J. Geophys. Res., 87, 6339–6345.

Huang, C. S. (2019a). Global ionospheric current system associated with penetration electric field and new mechanism for the generation of dayside westward electric field at low latitudes during northward IMF. J. Geophys. Res., Space Physics, 124, 3827–3842.

Huang, C. S. (2020). Systematical analyses of global ionospheric disturbance current systems caused by multiple processes: Penetration electric fields, solar wind pressure impulses, magnetospheric substorms, and ULF waves. J. Geophys. Res., Space Physics, 125, e2020JA027942. https://doi.org/10.1029/2020JA027942.

Huang, C.-S. (2009), Eastward electric field enhancement and geomagnetic positive bay in the dayside low-latitude ionosphere caused by magnetospheric substorms during sawtooth events, Geophys. Res. Lett., 36, L18102, doi:10.1029/2009GL040287.

Huang, C.-S. (2012), Statistical analysis of dayside equatorial ionospheric electric fields and electrojet currents produced by magnetospheric substorms during sawtooth events, J. Geophys. Res., 117, A02316, doi:10.1029/2011JA017398.

Hui, D., & Vichare, G. (2021). Influence of IMF-By on the equatorial ionospheric plasma drifts: TIEGCM simulations. J. Geophys. Res., Space Physics, 126, e2021JA029270. https://doi.org/10.1029/2021JA029270.

Iijima, T., &Potemra, T. A. (1978). Large-scale characteristics of field-aligned currents associated with substorms. J. Geophys. Res., 83(A2), 599–615.

Kelley, M. C., and J. J. Makela (2002). By dependent prompt penetrating electric fields at the magnetic equator. Geophys. Res. Lett., 29(7), 571–573, doi: 10.1029/2001GL014468.

Kelley, M. C., Fejer, B. G., & Gonzales, C. A. (1979). An explanation for anomalous equatorial ionospheric electric field associated with a northward turning of the interplanetary magnetic field. Geophys. Res. Lett., 6(4), 301–304.

Kelley, M. C., M. J. Nicolls, et al. (2007). Multi-longitude case studies comparing the interplanetary and equatorial ionospheric electric fields using an empirical model. J. Atmos. Terr. Phys., 69(10–11), 1174–1181, doi:10.1016/j.jastp.2006.08.014.

Kikuchi, T., H. Luhr, T. Kitamura, O. Saka, and K. Schlegel (1996). Direct penetration of the polar electric field to the equator during a DP2 event as detected by the auroral and equatorial magnetometer chains and the EISCAT radar. J. Geophys. Res., 101, 19,643.

Kikuchi, T., T. Araki, H. Maeda, and K. Maekawa (1978). Transmission of polar electric fields to the Equator. Nature, 273, 650–651.

Kumar, A., Chakrabarty, D., Fejer, B. G., Reeves, G. D., Rout, D., Sripathi, S., et al. (2023). A case of anomalous electric field perturbations in the equatorial ionosphere during post-sunset hours: insights, J. Geophys. Res., https://doi.org/10.1029/2022JA030826.

Lomb, N.R. (1976). Least-squares frequency analysis of unequally spaced data. Astrophys Space Sci 39, 447–462. https://doi.org/10.1007/BF00648343.

Mannucci, A. J., B. T. Tsurutani, B. A. Iijima, A. Komjathy, A. Saito, W. D. Gonzalez, F. L. Guarnieri, J. U. Kozyra, & R. Skoug (2005b). Dayside global ionospheric response to the major interplanetary events of October 29–30, 2003 “Halloween storms”. Geophys. Res. Lett., 32, L12S02, doi:10.1029/2004GL021467.

Nishida, A. (1968a). Geomagnetic DP 2 fluctuations and associated magnetospheric phenomena. J. Geophys. Res., 73(5), 1795–1803, doi: 10.1029/JA073i005p01795.

Nishida, A. (1968b). Coherence of geomagnetic DP 2 fluctuations with interplanetary magnetic variations. J. Geophys. Res., 73(17), 5549–5559, doi: 10.1029/JA073i017p05549.

Rout, D., Chakrabarty, D., Sekar, R., Reeves, G. D., Ruohoniemi, J. M., Pant, T. K., Veenadhari, B., & Shiokawa, K. (2016). An evidence for prompt electric field disturbance driven by changes in the solar wind density under northward IMF Bz condition. J. Geophys. Res., Space Physics, 121, 4800– 4810.

Rout, D., D. Chakrabarty, P. Janardhan, R. Sekar, V. Maniya, and K. Pandey (2017), Solar wind flow angle and geoeffectiveness of corotating interaction regions: First results, Geophys. Res. Lett., 44, 4532–4539.

Rout, D., Pandey, K., Chakrabarty, D., Sekar, R., & Lu, X. (2019). Significant electric field perturbations in low latitude ionosphere due to the passage of two consecutive ICMEs

during 6–8 September 2017. Journal of Geophysical Research: Space Physics, 124, 9494–9510.

Rout, D., R. Singh, K. Pandey, T.K. Pant, C. Stolle, D. Chakrabarty, S. Thampi, T. Bag, (2022). Evidence for Presence of a Global Quasi-Resonant Mode of Oscillations During High-Intensity Long-Duration Continuous AE Activity (HILDCAA) events, Earth, Planets and Space Express Letter, https://doi.org/10.1186/s40623-022-01642-1.

Rout, D., Kumar, A., Singh, R., Patra, S., Karan, D.K., Chakraborty, S., et al. (2025). Evidence of unusually strong equatorial ionization anomaly at three local time sectors during the Mother's Day geomagnetic storm on 10–11 May 2024. Geophys. Res. Lett., 52, e2024GL111269.

Ruohoniemi, J. M., & Greenwald, R. A. (2005). Dependencies of high-latitude plasma convection: Consideration of interplanetary magnetic field, seasonal, and universal time factors in statistical patterns. J. Geophys. Res., 110, A09204.

Sastri JH, Luhr H, Tachihara H, Kitamura T-I, Rao JVSV (2000). Electric field fluctuations (25 ± 35 min) in the midnight dip equatorial ionosphere. Ann Geophysicae 18:252 256.

Savitzky A, Golay MJ (1964). Smoothing and differentiation of data by simplified least squares procedures. Analyt Chem 36(8):1627–1639

Singh & Sripathi, S. (2021). The role of storm-time electrodynamics in the dawn and dusk sectors across equatorial and low-latitude ionosphere during December 19–21, 2015. J. Geophys. Res., Space Physics, 126, e2020JA029072.

Singh, R., Scipión, D. E., Kuyeng, K., Condor, P., De La Jara, C., Velasquez, J. P., et al. (2024). Ionospheric disturbances observed over the Peruvian sector during the Mother's Day Storm (G5-level) on 10–12 May 2024. J. Geophys. Res: Space Physics, 129, e2024JA033003.

Singh, R., Scipión, D. E., Kuyeng, K., Condor, P., Flores, R., Pacheco, E., et al. (2025). Ionospheric responses to an extreme (G5-level) geomagnetic storm using multi-instrument measurements at the Jicamarca Radio Observatory on 10–11 October 2024. J. Geophys. Res: Space Physics, 130, e2024JA033642.

Singh, R., Lee, Y.S. et al., (2022). Ionospheric density oscillations associated with recurrent prompt penetration electric fields during the space weather event of 4 November 2021 over the East-Asian sector. Journal of Geophysical Research: Space Physics, 127, e2022JA030456.

Tenfjord, P., Ostgaard, N.et al., (2015). How the IMF By induces a By component in the closed magnetosphere and how it leads to asymmetric currents and convection patterns in

the two hemispheres. J. Geophys. Res., 120, 9368–9384.

Torrence, C., & Compo, G. P. (1998). A practical guide to wavelet analysis. Bulletin of the American Meteorological Society, 79, 61–78. https://doi.org/10.1175/1520-0477.

Tsurutani, B. T., D. E. Jones, R. P. Lepping, E. J. Smith, and D. G. Sibeck (1984), The relationship between the IMF By and the distant tail (150–238 Re) lobe and plasma sheet By fields, Geophys. Res. Lett., 11, 1082.

Tsurutani, B. T., et al. (2008), Prompt penetration electric fields (PPEFs) and their ionospheric effects during the great magnetic storm of 30–31 October 2003, J. Geophys. Res., 113, A05311, doi:10.1029/2007JA012879.

Tsurutani, B., et al. (2004). Global dayside ionospheric uplift and enhancement associated with interplanetary electric fields. J. Geophys. Res., 109, A08302, doi:10.1029/2003JA010342.

Vasyliunas, V. M. (1989). Electrodynamics of the ionosphere/magnetosphere/solar wind system at high latitudes, in Electromagnetic Coupling in the Polar Clefts and Caps, edited by P. E. Sandholt and A. Egeland, p. 1, Springer, New York.

Vennerstrom, S., T. Moretto, et al. (2002). Field-aligned currents in the dayside cusp and polar cap region during northward IMF. J. Geophys. Res., 107(A8), 1188, doi: 10.1029/2001JA009162.

Wei, Y., Pu, Z., Hong, et al., (2009). Westward ionospheric electric field perturbations on the dayside associated with substorm processes. J. Geophys. Res., 114, A12209.

Weimer, D. R. (1995). Models of high-latitude electric potential derived with a least error fit of spherical harmonic coefficients. J. Geophys. Res., 100(A10), 19,595–19,607.

Weimer, D. R. (1996). A flexible, IMF-dependent model of high-latitude electric potential shaving “space weather” applications. Geophys. Res. Lett., 23(18), 2549–2552.

Zhang, K., Wang, H., Yamazaki, Y., & Xiong, C. (2021). Effects of subauroral polarization streams on the equatorial electrojet during the geomagnetic storm on June 1, 2013. Journal of Geophysical Research: Space Physics, 126, e2021JA029681. https://doi.org/10.1029/2021JA029681.

Figures

Figure 1. Solar wind and geomagnetic conditions on 19 December 2015. (a) X-component of the interplanetary magnetic field (IMF Bx); (b) Y- and Z-components of the IMF (By and Bz,

in nT); (c) Y-component of the interplanetary electric field (IEF Ey, in mV/m); (d) solar wind dynamic pressure (Pdyn, in nPa), proton density (Np, in cm^{-3}), and solar wind speed (Vsw, in km/s); (e) auroral electrojet indices (AU and AL, in nT); and (f) Sym-H index (in nT). The grey-shaded region highlights significant changes in the IMF Y-component between 16:30 and 18:00 UT.

Figure 2. Electron flux observations from the geosynchronous GOES satellites across multiple telescopes and energy channels. (a) GOES-13 and (b) GOES-15. The grey-shaded area indicates the time interval during which no significant changes in electron flux were observed.

Figure 3. Variations in the virtual height of the F-region (h'F) at (a) Guam (GUA), (b) Tirunelveli (TIR), and (c) Trivandrum (TVM); (d) vertical plasma drift (dh'F/dt) derived from h'F variations; (e) IMF Bz and By components. The grey lines with error bars represent the mean and standard deviation from five International Quiet Days (IQDs). The cyan-shaded region marks the period of significant ionospheric perturbations

Figure 4. (a–b) Variations in h'F at Fortaleza and Jicamarca; (c) vertical plasma drift from the Jicamarca ISR (JULIA, MP mode, shown as black circles) along with the Scherliess-Fejer (SF) model drift (black line); (d) equatorial electrojet (EEJ, green) along with the IQD mean and standard deviation (grey); and (e) IMF Bz (red), By (blue), and the detrended ΔEEJ (green). The grey-shaded region and vertical lines indicate periods of significant disturbances.

Figure 5. Periodogram analysis of IMF By, EEJ, and vertical plasma drift (dh'F/dt) over the Indian and American sectors. Left panels show the Lomb-Scargle (L-S) periodogram analysis, middle panels display the Morlet wavelet spectra, and right panels present the corresponding global wavelet spectra (GW).

Figure 6. SuperDARN ionospheric convection maps along with DP2 contours over the northern hemisphere on 19 December 2015, at (a) 17:00-17:02 and 17:06-17:08 UT (reverse convection; IMF By negative); (b) 17:18-17:20 and 17:20-17:22 UT (dusk cell rotation/expansion; IMF By positive); and (c) 17:26-17:28 and 17:30-17:32 UT (reverse convection; IMF By negative).

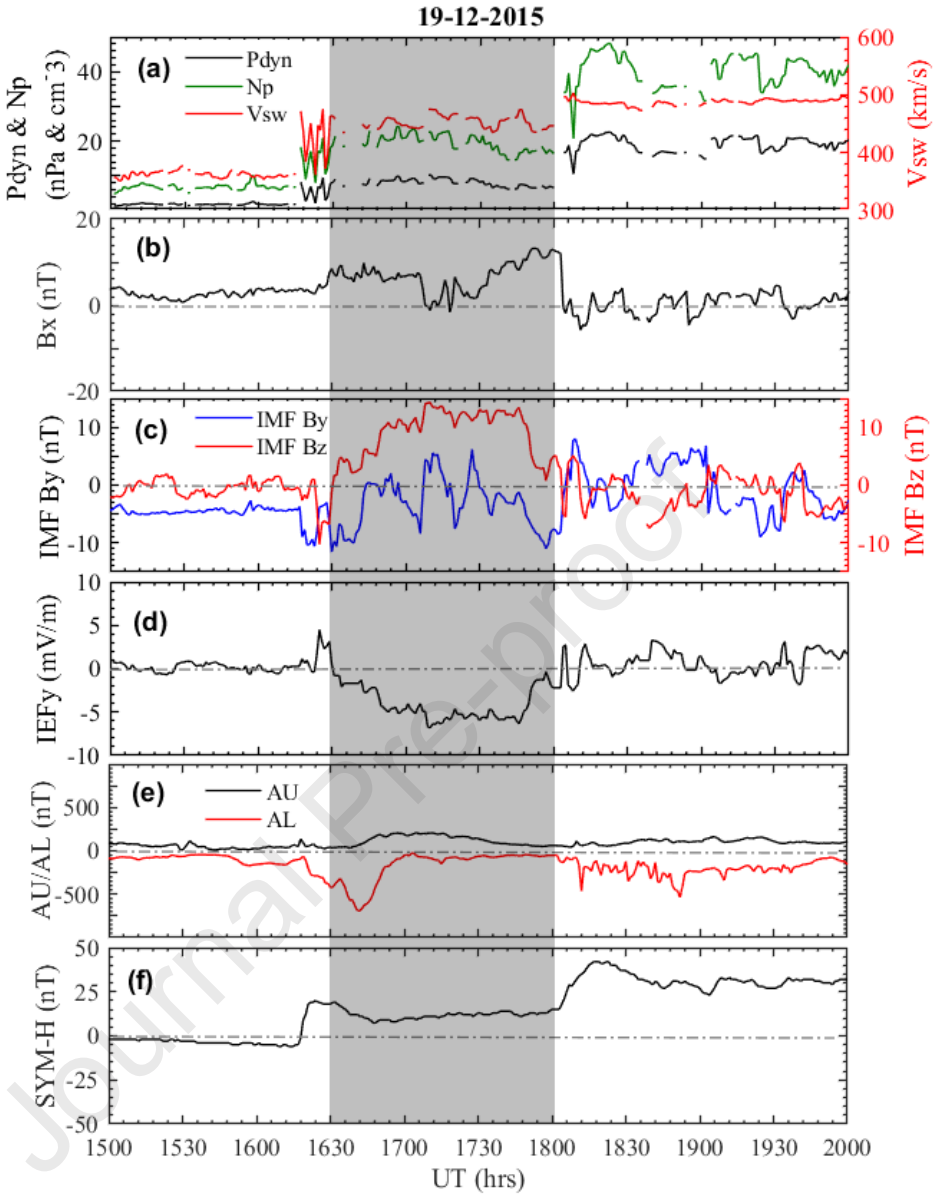
19-12-2015
(a)
Pdyn
Np
Vsw
Pdyn & Np (nPa & cm^-3)
Vsw (km/s)
(b)
Bx (nT)
(c)
IMF By
IMF Bz
IMF By (nT)
IMF Bz (nT)
(d)
IEFy (mV/m)
(e)
AU
AL
AU/AL (nT)
(f)
SYM-H (nT)
1500
1530
1600
1630
1700
1730
1800
1830
1900
1930
2000
UT (hrs)

Figure 1

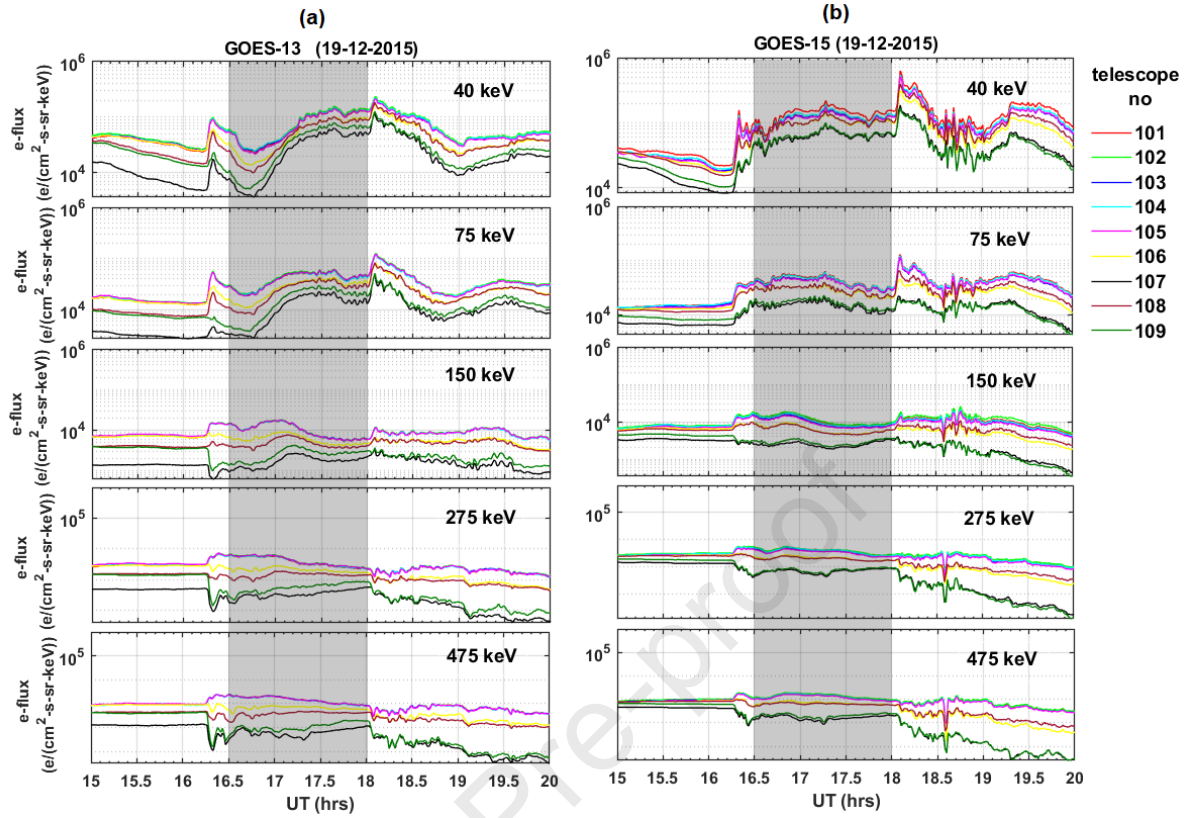

Figure 2

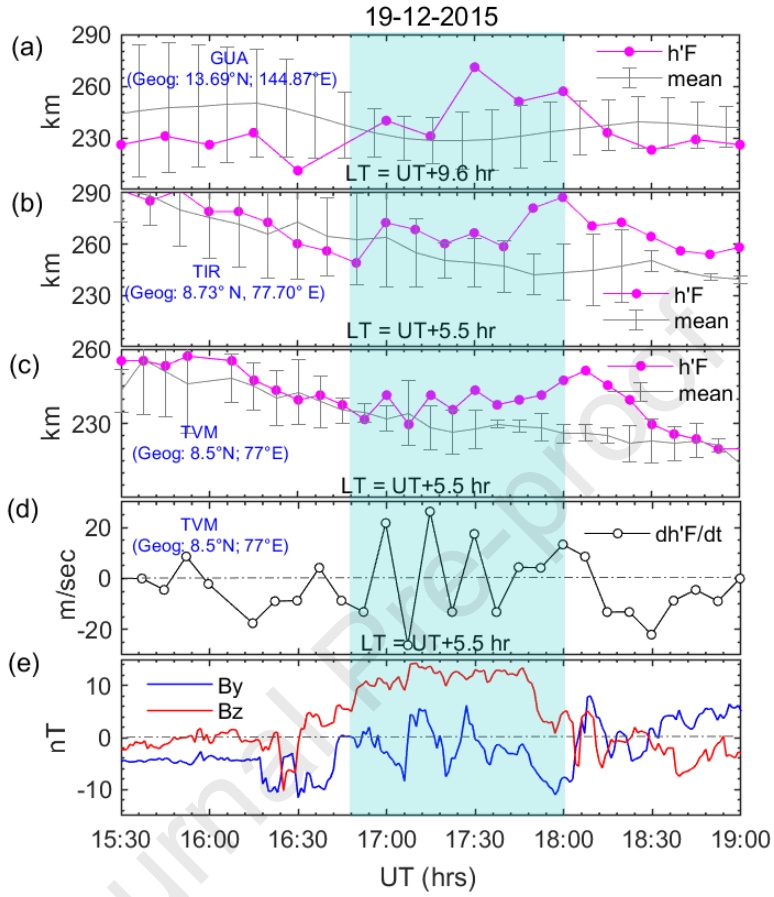
19-12-2015
(a)
GUA
(Geog: 13.69°N; 144.87°E)
h'F
mean
km
LT = UT+9.6 hr
(b)
TIR
(Geog: 8.73° N, 77.70° E)
h'F
mean
km
LT = UT+5.5 hr
(c)
TVM
(Geog: 8.5°N; 77°E)
h'F
mean
km
LT = UT+5.5 hr
(d)
TVM
(Geog: 8.5°N; 77°E)
dh'F/dt
m/sec
LT = UT+5.5 hr
(e)
By
Bz
nT
15:30
16:00
16:30
17:00
17:30
18:00
18:30
19:00
UT (hrs)

Figure 3

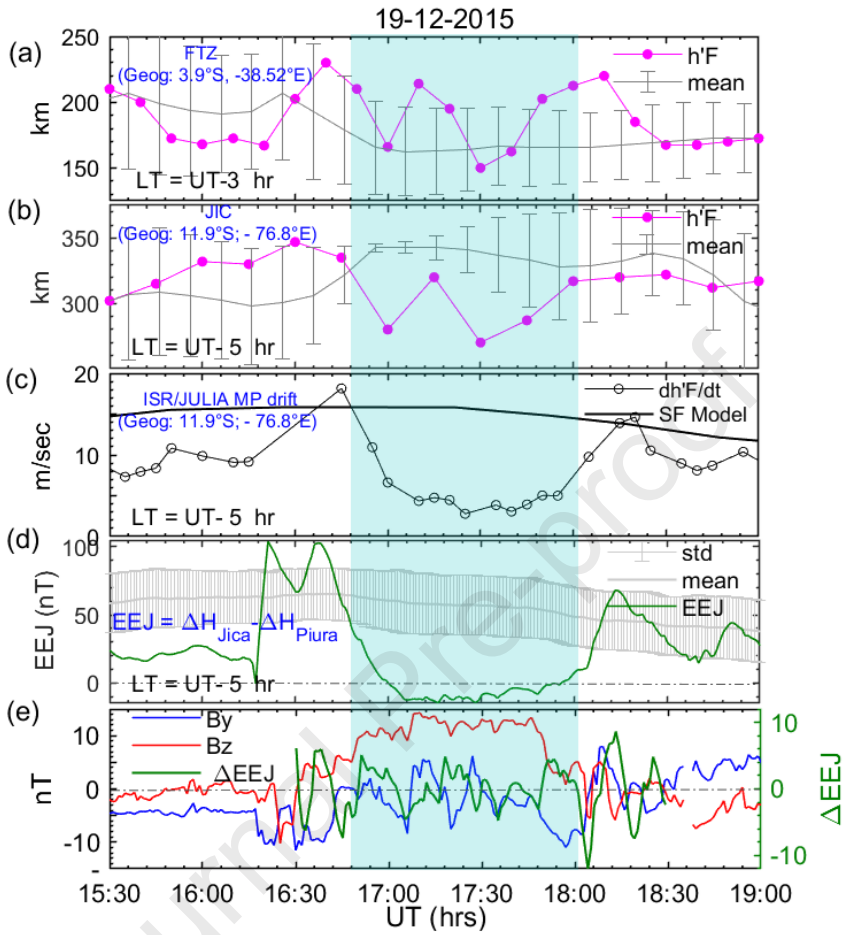
19-12-2015
(a)
FTZ
(Geog: 3.9°S, -38.52°E)
h'F
mean
km
LT = UT-3 hr
(b)
JIC
(Geog: 11.9°S; - 76.8°E)
h'F
mean
km
LT = UT- 5 hr
(c)
ISR/JULIA MP drift
(Geog: 11.9°S; - 76.8°E)
dh'F/dt
SF Model
m/sec
LT = UT- 5 hr
(d)
std
mean
EEJ
EEJ (nT)
EEJ = ΔH Jica -ΔH Piura
LT = UT- 5 hr
(e)
By
Bz
ΔEEJ
nT
ΔEEJ
15:30
16:00
16:30
17:00
17:30
18:00
18:30
19:00
UT (hrs)

Figure 4

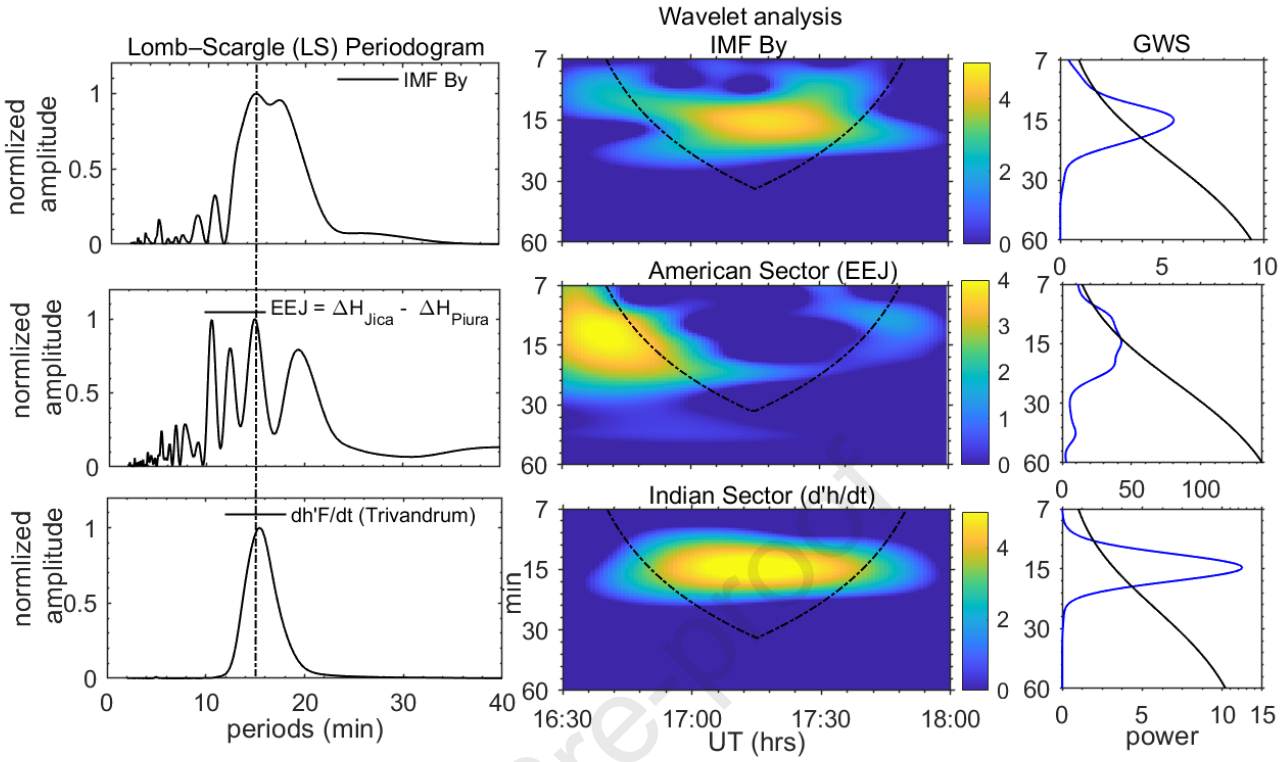

Figure 5

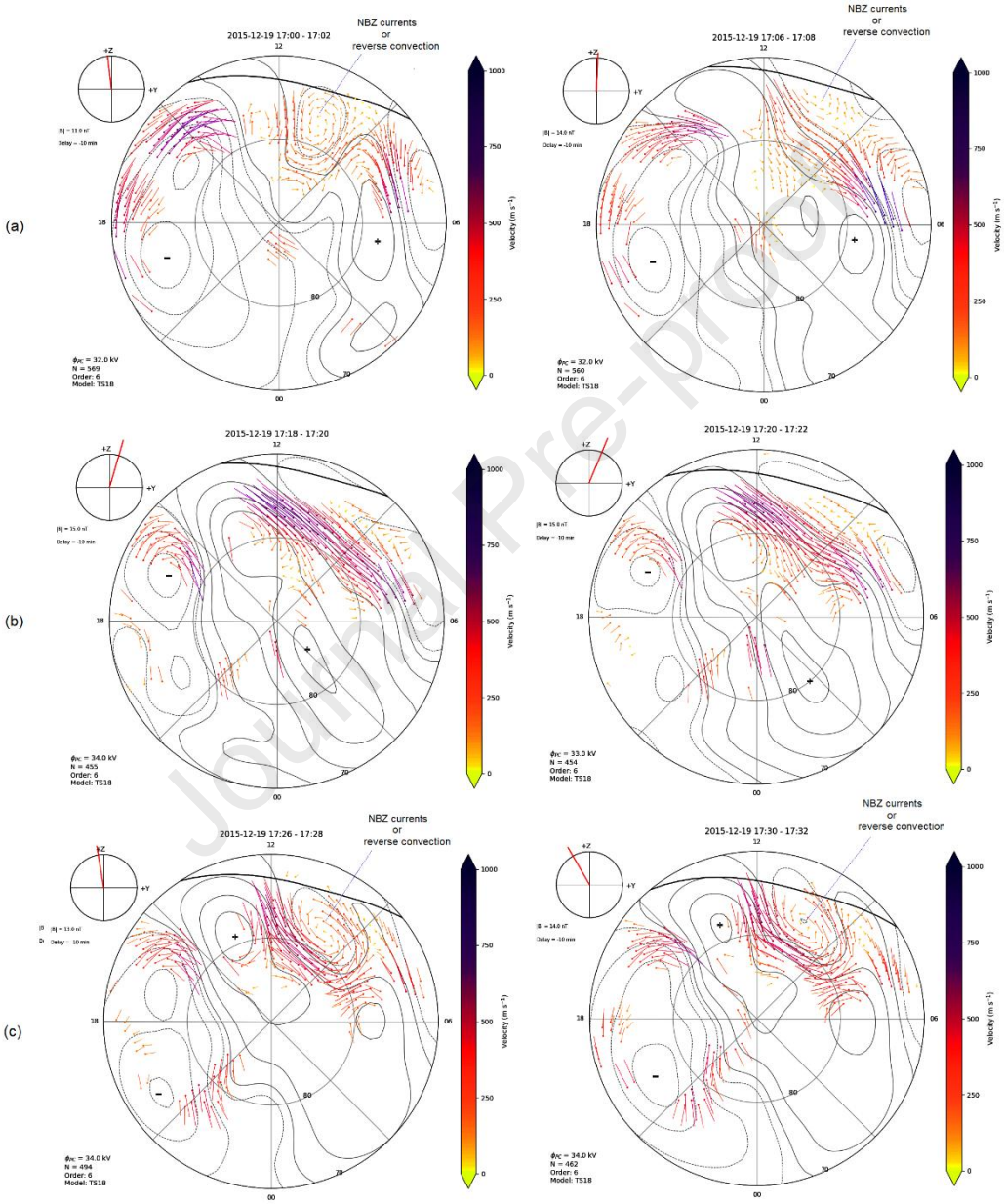
(a)
(b)
(c)
2015-12-19 17:00 - 17:02
2015-12-19 17:06 - 17:08
2015-12-19 17:18 - 17:20
2015-12-19 17:20 - 17:22
2015-12-19 17:26 - 17:28
2015-12-19 17:30 - 17:32
NBZ currents
or
reverse convection
Velocity (m s⁻¹)

Figure 6

1. Contrary to expectations, the same polarity penetration electric field observed at opposite longitudes during day and night local times.

2. IMF By-related quasi-periodic (~15 minutes) signature of penetration electric field.

3. Reverse convection and NBZ (northward Bz) currents cause an electric field with opposite polarity penetration to exist.

Declaration of Interest Statement

The authors declare that they have no known competing financial interests or personal relationships that could have appeared to influence the work reported in this paper